ETH zürich

ETH Library

Guanidinium-Formamidinium Lead Iodide: A Layered Perovskite-Related Compound with Red Luminescence at Room Temperature

Journal Article

Author(s):
Nazarenko, Olga; Kotyrba, Martin R.; Yakunin, Sergii; Aebli, Marcel; Rainò, Gabriele; Benin, Bogdan M.; Wörle, Michael; Kovalenko, Maksym V.

Publication date:
2018-03-21

Permanent link:
https://doi.org/10.3929/ethz-b-000254379

Rights / license:
In Copyright - Non-Commercial Use Permitted

Originally published in:
Journal of the American Chemical Society 140(11), https://doi.org/10.1021/jacs.8b00194

This page was generated automatically upon download from the ETH Zurich Research Collection.
For more information, please consult the Terms of use.

This is an open access article published under an ACS AuthorChoice License, which permits copying and redistribution of the article or any adaptations for non-commercial purposes.

JACS JOURNAL OF THE AMERICAN CHEMICAL SOCIETY

Communication

Cite This: J. Am. Chem. Soc. 2018, 140, 3850−3853

pubs.acs.org/JACS

Guanidinium-Formamidinium Lead Iodide: A Layered Perovskite-Related Compound with Red Luminescence at Room Temperature

Olga Nazarenko,[†,‡] Martin R. Kotyrba,[†,‡] Sergii Yakunin,[†,‡] Marcel Aebli,[†,‡] Gabriele Rainò,[†,‡] Bogdan M. Benin,[†,‡] Michael Wörle,[†] and Maksym V. Kovalenko*[,†,‡]

[†]Laboratory of Inorganic Chemistry, Department of Chemistry and Applied Bioscience, ETH Zürich, Vladimir Prelog Weg 1, CH-8093 Zürich, Switzerland

[‡]Laboratory for Thin Films and Photovoltaics, Empa − Swiss Federal Laboratories for Materials Science and Technology, Überlandstrasse 129, CH-8600 Dübendorf, Switzerland

Supporting Information

ABSTRACT: Two-dimensional hybrid organic−inorganic lead halides perovskite-type compounds have attracted immense scientific interest due to their remarkable optoelectronic properties and tailorable crystal structures. In this work, we present a new layered hybrid lead halide, namely $[CH(NH_2)_2][C(NH_2)_3]PbI_4$, wherein puckered lead-iodide layers are separated by two small and stable organic cations: formamidinium, $CH(NH_2)_2^+$, and guanidinium, $C(NH_2)_3^+$. This perovskite is thermally stable up to 255 °C, exhibits room-temperature photoluminescence in the red region with a quantum yield of 3.5%, and is photoconductive. This study highlights a vast structural diversity that exists in the compositional space typically used in perovskite photovoltaics.

Layered (two-dimensional, 2D) lead halide perovskites (LHPs) are unique, structurally soft and quantum-well-like systems, exhibiting enormous structural diversity[1] as well as high potential for applications in light emitting diodes,[2] photodetectors[3] or solar cells.[4] Most of 2D LHPs can be imagined as structural derivatives from the ideal cubic perovskite lattice of an $APbX_3$ composition [A, monovalent cation, primarily Cs^+, methylammonium (MA) or formamidinium (FA); X, halogen anion] with three-dimensional (3D) interconnection of corner-shared PbX_6-octahedra and with A-cations filling the large voids in-between these octahedra. Slicing of this lattice along (100), (110), (111) crystallographic planes (Figure 1) with the elimination of the octahedra lying in the slicing plane (gray-shaded octahedra in Figure 1) leads to common 2D-compounds with single-octahedra or thicker slabs. To induce the formation of 2D LHPs, A-site cations, which are typically used in 3D LHPs (Cs^+, MA, FA), must be fully or partially replaced with bulkier cations. (100)-layered 2D perovskites are most common and adopt K_2NiF_4 or $RbAlF_4$ crystal structure. As to (110)-2D LHPs ($Ca_2Nb_2O_7$ related phases), some known examples of A-cations include *N*-(3-aminopropyl)imidazolium [in $(C_6H_{13}N_3)PbBr_4$],[5] N^1-methyl-ethane-1,2-diammonium [N-MEDA, in $(N\text{-MEDA})PbBr_4$],[2a] as well as guanidinium [$C(NH_2)_3^+$, G, in G_2PbI_4].[6] An example of (111)-layered 2D LHP is the one comprising 3-(aminomethyl)-pyridinium [$(H_2\text{3-AMP})^{2+}$], such as in $(H_2\text{3-AMP})_2PbBr_6$ with K_2PtCl_6 type structure.[7] (100)-2D LHPs are most commonly built with primary mono and diammonium cations.[1g] The heavier the halide ion and the thicker the slab the smaller is the optical bandgap energy (E_g). As an example, in iodides, E_g varies from 2.57 eV in $(CH_3(CH_2)_3NH_3)_2PbI_4$[8] to 1.83 eV in $(CH_3(CH_2)_3NH_3)_2(CH_3NH_3)_4Pb_5I_{16}$.[9]

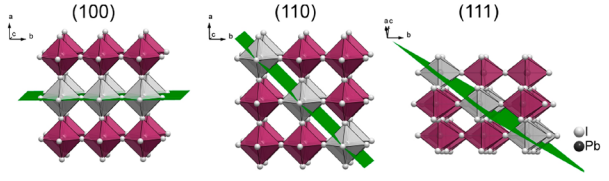

Figure 1. Derivation of 2D LHPs from the parental cubic perovskite lattice of 3D LHPs by cutting the latter along typical crystallographic planes: (100), (110), and (111).

Large Stokes shifts and broadband emission were recently reported for some (100) and (110) 2D-perovskites,[1b,2a,c,10] and were attributed to emission either from self-trapped excitons (STEx) or from charge carriers trapped on defects.[11]

Small and highly symmetric guanidinium cation forms a corrugated G_2PbI_4 structure with layers parallel to the (110) plane, and E_g of 2.40 eV.[6b] Smaller FA forms instead a 3D LHP, $FAPbI_3$ (α-phase, cubic symmetry),[12] with the smallest bandgap energy among all known LHPs, exhibiting PL maximum at 1.48 eV (to 840 nm in the near-infrared). α-$FAPbI_3$ is thermodynamically stable only above 185 °C,[13] whereas at room temperature (RT), α-$FAPbI_3$ undergoes a phase-transition into a wide-bandgap, nonluminescent 1D-polymorph (δ-$FAPbI_3$).[12,13] The ionic radii of FA and G cations are 253 and 278 pm, respectively.[14] The tolerance factor, a geometric parameter (α), introduced by V. M. Goldschmidt, describes a relation between the ionic radii (r_i) of A, B, X ions and a probability of a 3D perovskite lattice formation: $\alpha = (r_A + r_X)/\sqrt{2}(r_B + r_X)$.[14] Thus, when α = 0.9−1.0, formation of a cubic perovskite structure is favored and deviations from these values lead to distorted perovskites or nonperovskite, lower-dimensionality structures. While for $FAPbI_3$ α = 0.987, for $GPbI_3$ it increases to 1.039, causing crystallization in a 2D G_2PbI_4. Both FA and G ions are excellent

Received: January 6, 2018
Published: March 4, 2018

© 2018 American Chemical Society

DOI: 10.1021/jacs.8b00194
J. Am. Chem. Soc. 2018, 140, 3850−3853

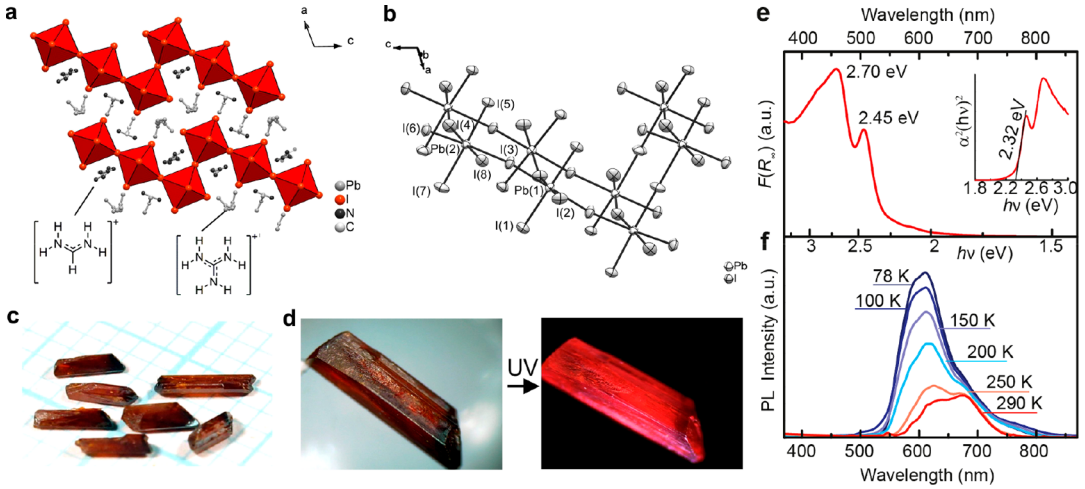

Figure 2. (a) Crystal structure of $FAGPbI_4$. (b) Octahedral coordination of lead ions. (c) A photograph of typical crystals (elipsoids shown at 50% probability). (d) Photographs of a $FAGPbI_4$ crystal taken under day light and under UV illumination in dark. (e) Kubelka–Munk function $F(R_\infty) = (1 - R_\infty)^2/2R_\infty$ (R_∞, diffusive reflectance) and (f) temperature-dependent PL spectra measurements performed on powdered crystals.

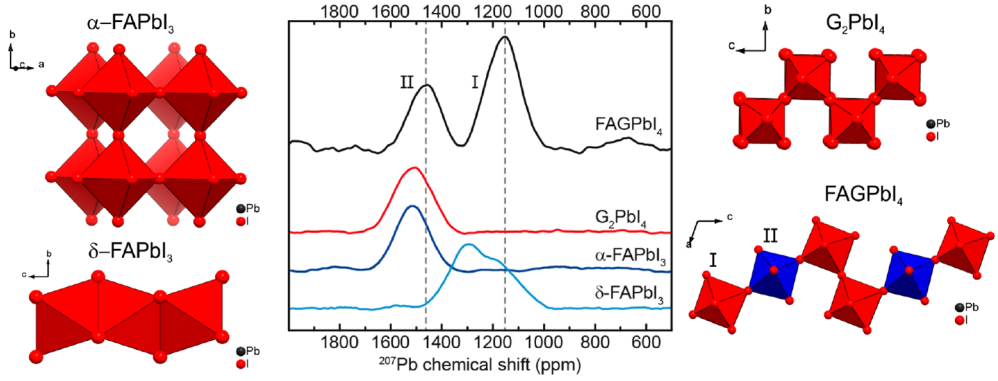

Figure 3. ^{207}Pb ssNMR spectra of $FAGPbI_4$, G_2PbI_4, α-$FAPbI_3$ and δ-$FAPbI_3$. All spectra were acquired under 20 kHz magic-angle spinning, except for α-$FAPbI_3$, which was recorded in static mode.

donors of hydrogen bonds with the lead-halide framework. It is thus of high interest to explore the possibility of concomitant incorporation of FA and G for the formation of previously unknown compounds. These compounds might exhibit reduced volume of the interlayer region as compared to G-only or larger-cation compounds. Such compactness and resulting reduction of E_g had been shown in previous studies on Cs^+/G and on MA/G systems.[15] G and similar ions are increasingly used as additives to MA/FA/Cs-based $APbX_3$ compounds in perovskite photovoltaics.[16] Hence, the search for structural motifs within this compositional space is highly relevant for understanding perovskite optoelectronic devices.

In this work, a new 2D perovskite with a crystal structure composed of corrugated inorganic layers, $[CH(NH_2)_2][C(NH_2)_3]PbI_4$ (Figure 2a–c) further denoted also as $FAGPbI_4$, was identified in the FA-G-PbI_2 system. Such layered network can be visualized as stair-like slabs of corner-sharing Pb–I octahedra (Figure 2). It shows broadband emission in the red region at RT (Figure 2d) that originates from both free and self-trapped excitons.

$FAGPbI_4$ was crystallized from hydroiodic acid as 0.5–3 mm long needles (Figure 2c, see Supporting Information, SI, for further details). Briefly, FA acetate (4 mmol), G_2CO_3 (4 mmol) and lead acetate trihydrate (4 mmol) were dissolved in 18 mL of aqueous HI (57% by mass) upon moderate heating (~50 °C). After cooling to RT, the solution was left undisturbed for 1–2 days to allow crystallization of $FAGPbI_4$. Crystals were isolated by vacuum filtration and purified by washing with diethyl ether and toluene. The purity of $FAGPbI_4$ was confirmed by powder X-ray diffraction (pXRD) and the thermal stability was studied with thermogravimetric analysis and differential scanning calorimetry (Figure S1). $FAGPbI_4$ crystallizes in a monoclinic crystal system (space group $C2/m$, Table S1). The crystal structure is composed of corrugated Pb–I layers and G and FA cations situated in the interlayer space (Figure 2a,b). Interestingly, in comparison with a related compound G_2PbI_4 (included in Figure 3), composed of zigzag Pb–I layers,[2c] $FAGPbI_4$ shows stair-like corrugation of inorganic layers. Concomitant use of FA and G ions in a lead iodide system results in a different crystal structure as compared to MA-G-PbI_2 and Cs-G-PbI_2 systems, where Ruddlesden–Popper-like phases form (Figure S2).[15] The crystal structure of $FAGPbI_4$ had been deposited as a CIF file into the CCDC database with the number 1814744.

In general, the bandgap energy is determined by such factors as the dimensionality, connectivity of the structure and distortions of the coordination polyhedra (lengths of the Pb–X bonds and Pb–X–Pb angles), as well the atomic number of the halide.[17] In $FAGPbI_4$, Pb–I distances lie in the range of 3.080(1)–3.361(1) Å and are comparable to those in G_2PbI_4

DOI: 10.1021/jacs.8b00194
J. Am. Chem. Soc. 2018, 140, 3850–3853

[d(Pb–I) = 3.070(14)–3.362(14) Å].[6a] I–Pb–I bond angles in $FAGPbI_4$ deviate from 90° and are in the range of 86.36(3)–95.66(2)°; Pb–I–Pb angles range from 161.98° to 180°. In comparison, Pb–I–Pb angles in G_2PbI_4 are in the range of 156.9–177.5°. The complete set of bond distances and bond angles can be found in Tables S2–S4. The optical absorption spectrum of powdered $FAGPbI_4$ is represented here by the Kubelka–Munk function $F(R_\infty) = \alpha/S = (1 - R_\infty)^2/2R_\infty$, where α is an absorption coefficient, S is a scattering coefficient and R_∞ is a reflectance of an infinitely thick layer. The absorption transitions appear at 506 and 459 nm (Figure 2e, S3), with only a weak absorbance below 620 nm. The compound exhibits red PL under UV excitation at RT (Figure 2d), which is a spectrally broad convolution of several bands (Figure 2f). At RT, the PL quantum yield (PLQY) reaches 3.5%, when excited in the wavelength range of 550–600 nm and drops to about 1% for the excitation at wavelengths shorter than 500 nm (Figure S4).

Solid-state nuclear magnetic resonance spectroscopy (ssNMR, in standard magic-angle spinning version) had been used to characterize $FAGPbI_4$ and to delineate whether the PL originates from amorphous/nanocrystalline contaminants, not detectable by pXRD. The high purity of $FAGPbI_4$ was confirmed by comparing its ^{207}Pb ssNMR spectrum with the spectra of plausible contaminants: G_2PbI_4, α-$FAPbI_3$ and δ-$FAPbI_3$ (see NMR and XRD data in Figures 3 and S5–S7). $FAGPbI_4$ exhibits two peaks, at 1160 and 1465 ppm (referenced to $PbMe_4$), with a full width at half-maximum (fwhm) of 22.4 and 20.2 kHz, respectively, which are typical values for inorganic lead(II)-iodide compounds[18] and LHPs.[19] The ratio of the peak areas of 2:1 corresponds to the staggered crystal structure. ^{207}Pb ssNMR spectra of G_2PbI_4 and α-$FAPbI_3$ exhibit single peaks at 1515 ppm. The narrower signal of α-$FAPbI_3$ (fwhm = 22.2 kHz), as compared to G_2PbI_4 (fwhm = 24.5 kHz), can be attributed to the higher symmetry and rigidity of the former structure. In contrast, δ-$FAPbI_3$ shows a complex spectrum with spinning side bands. The isotropic chemical shift was determined by varying the MAS spinning frequency and, after deconvolution, was found to be −1175 ppm with a fwhm of 21.8 kHz (Figure S8). This spectrum indicates a larger asymmetry of the Pb environment in δ-$FAPbI_3$. None of the other plausible impurities such as precursors (e.g., lead acetate) or side products (PbI_2, $PbCO_3$, PbO or Pb(OH)I, etc.) could be detected by sampling a broader range of chemical shifts (Figures S9).

Understanding of the broadband emission from layered LHPs is nontrivial due to effects of the increased structural dynamics in their soft lattices. Temperature-dependent PL measurements were taken to further investigate the complexity of the PL from $FAGPbI_4$ (Figure 2f). With cooling, higher-energy emission shifts to shorter wavelength, up to around 600 nm at 78 K and notably grows in intensity, as one would expect from the excitonic emission.

The longer-wavelength side of the PL envelope is much less altered by the temperature. Time-resolved measurements also point to distinctly different nature of lower and higher energy emission bands (Figure 4). Two spectral regions were probed; these were defined through the use of short- and long-pass optical filters, as indicated by shaded areas. Typically, structurally rigid 2D LHP structures exhibit narrow-band PL with short lifetimes for excitonic transitions, from a few to tens of ns, whereas more complex structures with STEx are characterized by broader emission with one-to-2 orders of magnitude longer lifetimes.[2c,20] Minor changes in average lifetime for 500–650 nm spectral region as a function of the excitation intensity was observed, as opposed to the region of 700–750 nm, characterized by much stronger power dependence (Figure S10). At 700–750 nm, the PL lifetime decreases with the increase of excitation power. While still speculative, the PL band at ca. 645 nm can be attributed to (near) band-edge excitons, whereas lower-energy emission (at around 685 nm) might be STEx-related. However, for the lower-energy emission band, we cannot exclude that the emission can also be related to defects or color centers.[21] All decay traces are multi-exponential and are compared by their average lifetimes (τ_{avg}, extracted from biexponential fits). The lower-energy PL is characterized by long τ_{avg} on the order of hundreds of ns, which increases with increasing the temperature. Considering that the PL QYs are on the order of a few %, it is impossible to unambiguously assign these lifetimes to exclusively radiative processes. Additional measurements, such as spectral dependences of PL excitation and PLQYs, excitation power dependent time-resolved PL (TRPL), and TRPL with micrometer spatial resolution (see Figures S3, S4, S10, S11), do not allow for a more accurate assignment of the complex and overlapping emission bands in such 2D LHPs.

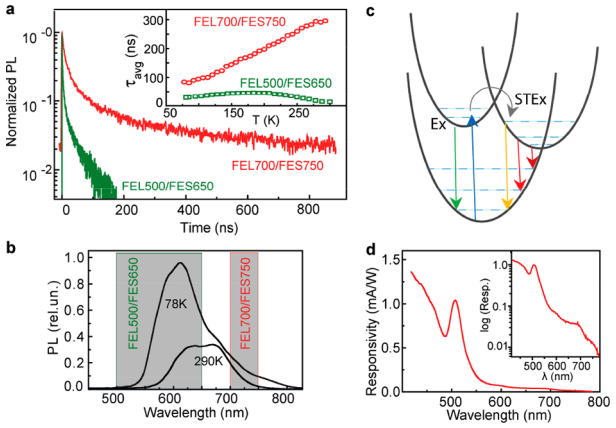

Figure 4. (a) RT time-resolved PL traces recorded in two spectral ranges (indicated in panel b) : 500–650 nm (green) and 700–750 nm (red). Inset: temperature-dependence of the average PL lifetime. (c) Configuration coordinate diagram for free excitons and STEx. (d) Photoconductivity spectrum from a single $FAGPbI_4$ crystal.

The extended 2D electronic structure of $FAGPbI_4$ allows for the observation of photoconductivity (Figure 4d). The dark specific resistivity values were ca. 1×10^{10} Ω·cm, indicating rather low intrinsic carrier concentration and/or mobility. The photoconductivity spectrum of a single $FAGPbI_4$ crystal peaks at 510 nm, coinciding with the absorption peak in the Kubelka–Munk function. The tail of the weak photoconductivity extends to 700 nm, thus covering the range in which PL bands are observed. Again, as in the case of PL, it remains impossible to disentangle two possible origins of this photoconductivity: from trap states or from STEx. Furthermore, we note that the fine spectral details of the PL vary also with the synthesis method (see methods 1 and 2, and Figure S12 in SI for more details).

In conclusion, a new layered compound, $FAGPbI_4$, is thermally stable until 255 °C, exhibits PL at RT and pronounced photoconductivity. This study highlights a plethora of structures, other than traditional ABX_3 LHPs, that can form

DOI: 10.1021/jacs.8b00194
J. Am. Chem. Soc. 2018, 140, 3850–3853

in the compositional space comprising Cs^+, FA, MA, G as A-site cations or interlayer cations.

■ ASSOCIATED CONTENT

Supporting Information

The Supporting Information is available free of charge on the ACS Publications website at DOI: 10.1021/jacs.8b00194.

Data for $[CH(NH_2)][C(NH_2)_3]PbI_4$ (i.e., $FAGPbI_4$) (CIF)

Crystallographic data for $FAGPbI_4$ and additional characterization (PDF)

■ AUTHOR INFORMATION

Corresponding Author

*mvkovalenko@ethz.ch

ORCID

Sergii Yakunin: 0000-0002-6409-0565

Maksym V. Kovalenko: 0000-0002-6396-8938

Notes

The authors declare no competing financial interest.

■ ACKNOWLEDGMENTS

This work was financially supported by the European Union through the FP7 (ERC Starting Grant NANOSOLID, GA No. 306733) and through the Horizon-2020 (Marie-Skłodowska Curie ITN network PHONSI, H2020-MSCA-ITN-642656).

■ REFERENCES

(1) (a) Mitzi, D. B.; Chondroudis, K.; Kagan, C. R. *IBM J. Res. Dev.* **2001**, *45*, 29−45. (b) Dohner, E. R.; Jaffe, A.; Bradshaw, L. R.; Karunadasa, H. I. *J. Am. Chem. Soc.* **2014**, *136*, 13154−13157. (c) Stoumpos, C. C.; Cao, D. H.; Clark, D. J.; Young, J.; Rondinelli, J. M.; Jang, J. I.; Hupp, J. T.; Kanatzidis, M. G. *Chem. Mater.* **2016**, *28*, 2852−2867. (d) Stoumpos, C. C.; Soe, C. M. M.; Tsai, H.; Nie, W.; Blancon, J.-C.; Cao, D. H.; Liu, F.; Traoré, B.; Katan, C.; Even, J.; Mohite, A. D.; Kanatzidis, M. G. *Chem.* **2017**, *2*, 427−440. (e) Smith, M. D.; Watson, B. L.; Dauskardt, R. H.; Karunadasa, H. I. *Chem. Mater.* **2017**, *29*, 7083−7087. (f) Smith, M. D.; Jaffe, A.; Dohner, E. R.; Lindenberg, A. M.; Karunadasa, H. I. *Chem. Sci.* **2017**, *8*, 4497−4504. (g) Saparov, B.; Mitzi, D. B. *Chem. Rev.* **2016**, *116*, 4558−4596. (h) Mitzi, D. B. *Synthesis, structure, and properties of organic-inorganic perovskites and related materials*; John Wiley & Sons, Inc., 1999.

(2) (a) Dohner, E. R.; Hoke, E. T.; Karunadasa, H. I. *J. Am. Chem. Soc.* **2014**, *136*, 1718−1721. (b) Dohner, E. R.; Jaffe, A.; Bradshaw, L. R.; Karunadasa, H. I. *J. Am. Chem. Soc.* **2014**, *136*, 13154−13157. (c) Mao, L.; Wu, Y.; Stoumpos, C. C.; Wasielewski, M. R.; Kanatzidis, M. G. *J. Am. Chem. Soc.* **2017**, *139*, 5210−5215.

(3) (a) Li, L.; Sun, Z.; Wang, P.; Hu, W.; Wang, S.; Ji, C.; Hong, M.; Luo, J. *Angew. Chem.* **2017**, *129*, 12318−12322. (b) Tan, Z.; Wu, Y.; Hong, H.; Yin, J.; Zhang, J.; Lin, L.; Wang, M.; Sun, X.; Sun, L.; Huang, Y.; Liu, K.; Liu, Z.; Peng, H. *J. Am. Chem. Soc.* **2016**, *138*, 16612−16615.

(4) (a) Tsai, H.; Nie, W.; Blancon, J.-C.; Stoumpos, C. C.; Asadpour, R.; Harutyunyan, B.; Neukirch, A. J.; Verduzco, R.; Crochet, J. J.; Tretiak, S.; Pedesseau, L.; Even, J.; Alam, M. A.; Gupta, G.; Lou, J.; Ajayan, P. M.; Bedzyk, M. J.; Kanatzidis, M. G.; Mohite, A. D. *Nature* **2016**, *536*, 312−316. (b) Smith, I. C.; Hoke, E. T.; Solis-Ibarra, D.; McGehee, M. D.; Karunadasa, H. I. *Angew. Chem., Int. Ed.* **2014**, *53*, 11232−11235.

(5) Li, Y. Y.; Lin, C. K.; Zheng, G. L.; Cheng, Z. Y.; You, H.; Wang, W. D.; Lin, J. *Chem. Mater.* **2006**, *18*, 3463−3469.

(6) (a) Szafrański, M.; Stahl, K. *Phys. Rev. B: Condens. Matter Mater. Phys.* **2000**, *62*, 8787. (b) Hillebrecht, H.; Daub, M.; Haber, C. *Eur. J. Inorg. Chem.* **2017**, *2017*, 1120−1126.

(7) Li, Y.; Zheng, G.; Lin, C.; Lin, J. *Solid State Sci.* **2007**, *9*, 855−861.

(8) Ishihara, T. *J. Lumin.* **1994**, *60*, 269−274.

(9) Stoumpos, C. C.; Malliakas, C. D.; Kanatzidis, M. G. *Inorg. Chem.* **2013**, *52*, 9019−9038.

(10) Yangui, A.; Garrot, D.; Lauret, J. S.; Lusson, A.; Bouchez, G.; Deleporte, E.; Pillet, S.; Bendeif, E. E.; Castro, M.; Triki, S.; Abid, Y.; Boukheddaden, K. *J. Phys. Chem. C* **2015**, *119*, 23638−23647.

(11) Hu, T.; Smith, M. D.; Dohner, E. R.; Sher, M.-J.; Wu, X.; Trinh, M. T.; Fisher, A.; Corbett, J.; Zhu, X. Y.; Karunadasa, H. I.; Lindenberg, A. M. *J. Phys. Chem. Lett.* **2016**, *7*, 2258−2263.

(12) Weller, M. T.; Weber, O. J.; Frost, J. M.; Walsh, A. *J. Phys. Chem. Lett.* **2015**, *6*, 3209−3212.

(13) Han, Q.; Bae, S.-H.; Sun, P.; Hsieh, Y.-T.; Yang, Y.; Rim, Y. S.; Zhao, H.; Chen, Q.; Shi, W.; Li, G.; Yang, Y. *Adv. Mater.* **2016**, *28*, 2253−2258.

(14) Kieslich, G.; Sun, S.; Cheetham, A. K. *Chem. Sci.* **2014**, *5*, 4712−4715.

(15) (a) Nazarenko, O.; Kotyrba, M. R.; Wörle, M.; Cuervo-Reyes, E.; Yakunin, S.; Kovalenko, M. V. *Inorg. Chem.* **2017**, *56*, 11552−11564. (b) Soe, C. M. M.; Stoumpos, C. C.; Kepenekian, M.; Traoré, B.; Tsai, H.; Nie, W.; Wang, B.; Katan, C.; Seshadri, R.; Mohite, A. D.; Even, J.; Marks, T. J.; Kanatzidis, M. G. *J. Am. Chem. Soc.* **2017**, *139*, 16297−16309.

(16) (a) Jodlowski, A. D.; Roldán-Carmona, C.; Grancini, G.; Salado, M.; Ralaiarisoa, M.; Ahmad, S.; Koch, N.; Camacho, L.; de Miguel, G.; Nazeeruddin, M. K. *Nat. Energy* **2017**, *2*, 972−979. (b) Correa-Baena, J.-P.; Saliba, M.; Buonassisi, T.; Grätzel, M.; Abate, A.; Tress, W.; Hagfeldt, A. *Science* **2017**, *358*, 739−744.

(17) (a) Stoumpos, C. C.; Kanatzidis, M. G. *Acc. Chem. Res.* **2015**, *48*, 2791−2802. (b) Lemmerer, A.; Billing, D. G. *Dalton Trans.* **2012**, *41*, 1146−1157.

(18) (a) Kye, Y.-S.; Connolly, S.; Herreros, B.; Harbison, G. S. *Main Group Met. Chem.* **1999**, *22*, 373−383. (b) Dybowski, C.; Smith, M. L.; Hepp, M. A.; Gaffney, E. J.; Neue, G.; Perry, D. L. *Appl. Spectrosc.* **1998**, *52*, 426−429. (c) Taylor, R.; Beckmann, P. A.; Bai, S.; Dybowski, C. *J. Phys. Chem. C* **2014**, *118*, 9143−9153.

(19) (a) Rosales, B. A.; Men, L.; Cady, S. D.; Hanrahan, M. P.; Rossini, A. J.; Vela, J. *Chem. Mater.* **2016**, *28*, 6848−6859. (b) Roiland, C.; Trippé-Allard, G.; Jemli, K.; Alonso, B.; Ameline, J.-C.; Gautier, R.; Bataille, T.; Le Polles, L.; Deleporte, E.; Even, J.; et al. *Phys. Chem. Chem. Phys.* **2016**, *18*, 27133−27142.

(20) (a) Kitazawa, N.; Aono, M.; Watanabe, Y. *Thin Solid Films* **2010**, *518*, 3199−3203. (b) Kitazawa, N.; Aono, M.; Watanabe, Y. *J. Phys. Chem. Solids* **2011**, *72*, 1467−1471.

(21) Booker, E. P.; Thomas, T. H.; Quarti, C.; Stanton, M. R.; Dashwood, C. D.; Gillett, A. J.; Richter, J. M.; Pearson, A. J.; Davis, N. J. L. K.; Sirringhaus, H.; Price, M. B.; Greenham, N. C.; Beljonne, D.; Dutton, S. E.; Deschler, F. *J. Am. Chem. Soc.* **2017**, *139*, 18632−18639.

DOI: 10.1021/jacs.8b00194
J. Am. Chem. Soc. 2018, 140, 3850−3853